

2009

# Contribution of a Portable Air Plasma Torch to Rapid Blood Coagulation as a Method of Preventing Bleeding

Kuo S. P.

O. Tarasenko


J. Chang

S. Popović

C. Y. Chen

*See next page for additional authors*

Follow this and additional works at: <http://repository.usfca.edu/phys>

 Part of the [Analytical, Diagnostic and Therapeutic Techniques and Equipment Commons](#), and the [Physics Commons](#)

---

## Recommended Citation

Kuo, S.P., Tarasenko, O., Chang, J., Popovic, S., Chen, C.Y., Fan, H.W., Scott, A., Lahiani, M., Alusta, P., Drake, J.D., Nikolic, M. Contribution of a portable air plasma torch to rapid blood coagulation as a method of preventing bleeding. (2009) *New Journal of Physics*, 11, art. no. 115016. <http://dx.doi.org/10.1088/1367-2630/11/11/115016>

This Article is brought to you for free and open access by the College of Arts and Sciences at USF Scholarship: a digital repository @ Gleeson Library | Geschke Center. It has been accepted for inclusion in Physics and Astronomy by an authorized administrator of USF Scholarship: a digital repository @ Gleeson Library | Geschke Center. For more information, please contact [repository@usfca.edu](mailto:repository@usfca.edu).

---

**Authors**

Kuo S. P., O. Tarasenko, J. Chang, S. Popović, C. Y. Chen, H. W. Fan, A. Scott, M. Lahiani, P. Alusta, J. D. Drake, and Milka Nikolic

## Contribution of a portable air plasma torch to rapid blood coagulation as a method of preventing bleeding

This content has been downloaded from IOPscience. Please scroll down to see the full text.

2009 New J. Phys. 11 115016

(<http://iopscience.iop.org/1367-2630/11/11/115016>)

View [the table of contents for this issue](#), or go to the [journal homepage](#) for more

Download details:

IP Address: 138.202.1.218

This content was downloaded on 25/04/2017 at 22:13

Please note that [terms and conditions apply](#).

You may also be interested in:

[Plasma effects on bacterial spores in a wet environment](#)

Spencer P Kuo, Olga Tarasenko, Said Nourkbash et al.

[Fan-shaped plasma for mail decontamination](#)

Spencer P Kuo, S Popovic, Olga Tarasenko et al.

[Plasma medicine: an introductory review](#)

M G Kong, G Kroesen, G Morfill et al.

[Spectroscopy of reactive species produced by low-energy atmospheric-pressure plasma on conductive target material surface](#)

Hiromasa Yamada, Hajime Sakakita, Susumu Kato et al.

[Optical diagnostics of a low power—low gas flow rates atmospheric-pressure argon plasma created by a microwave plasma torch](#)

Chuji Wang, Nimisha Srivastava, Susan Scherrer et al.

[Atmospheric-pressure plasma sources for biomedical applications](#)

G Y Park, S J Park, M Y Choi et al.

[Generation and transport mechanisms of chemical species by a post-discharge flow for inactivation of bacteria](#)

Takehiko Sato, Shiroh Ochiai and Takuya Urayama

[Reduction and degradation of amyloid aggregates by a pulsed radio-frequency cold atmospheric plasma jet](#)

D L Bayliss, J L Walsh, G Shama et al.

## Contribution of a portable air plasma torch to rapid blood coagulation as a method of preventing bleeding

S P Kuo<sup>1,5</sup>, O Tarasenko<sup>2,5</sup>, J Chang<sup>3</sup>, S Popovic<sup>4</sup>, C Y Chen<sup>1</sup>,  
H W Fan<sup>1</sup>, A Scott<sup>2</sup>, M Lahiani<sup>2</sup>, P Alusta<sup>2</sup>, J D Drake<sup>4</sup>  
and M Nikolic<sup>4</sup>

<sup>1</sup> Department of Electrical and Computer Engineering, Polytechnic Institute of New York University, Brooklyn, NY 11201, USA

<sup>2</sup> Department of Biology, University of Arkansas at Little Rock, Little Rock, AR 72204, USA

<sup>3</sup> Department of Radiation Oncology, New York University School of Medicine, New York, NY 10016, USA

<sup>4</sup> Department of Physics, Old Dominion University, Norfolk, VA 23529, USA  
E-mail: [skuo@duke.poly.edu](mailto:skuo@duke.poly.edu)

*New Journal of Physics* **11** (2009) 115016 (17pp)

Received 29 June 2009

Published 26 November 2009

Online at <http://www.njp.org/>

doi:10.1088/1367-2630/11/11/115016

**Abstract.** The effectiveness and mechanism of a low temperature air plasma torch in clotting blood are explored. Both blood droplets and smeared blood samples were used in the tests. The treated droplet samples reveal how blood clotting depends on the distance at which the torch operated, and for how long the droplets have been exposed to the torch. Microscopy and cell count of smeared blood samples shed light on dependencies of erythrocyte and platelet counts on torch distance and exposure time. With an increase of torch distance, the platelet count of treated blood samples increases but is less than that of the control. The flux of reactive atomic oxygen (RAO) and the degree of blood clotting decreased. With an increase of exposure time, platelet count of treated samples decreased, while the degree of clot increased. The correlation among these dependencies and published data support a blood clotting mechanism that RAO as well as other likely reactive oxygen species generated by the plasma torch activate erythrocyte–platelets interactions and induces blood coagulation.

<sup>5</sup> These authors contributed equally to this study.

**Contents**

<b>1. Introduction</b>	<b>2</b>
<b>2. Portable APT</b>	<b>3</b>
2.1. Physical and electric characteristics . . . . .	3
2.2. Temperature measurements . . . . .	4
2.3. Emission spectroscopy . . . . .	6
<b>3. Preparations</b>	<b>8</b>
3.1. Materials . . . . .	8
3.2. Preparations prior to plasma exposure . . . . .	8
3.3. Experimental setup . . . . .	9
3.4. Microscopy of plasma treated samples . . . . .	9
<b>4. Experiments</b>	<b>10</b>
<b>5. Coagulation mechanism</b>	<b>11</b>
<b>6. Discussion</b>	<b>14</b>
<b>Acknowledgments</b>	<b>15</b>
<b>References</b>	<b>15</b>

**1. Introduction**

Hemorrhage is defined as bleeding or an abnormal flow of blood [1]–[4]. Hemorrhages are classified as internal, external, or a combination of both. Internal hemorrhage usually goes unnoticed (for instance bleeding into the spleen, liver, bleeding during malignancy, stroke, or post-surgery). Bleeding from a cut on the skin is considered an external hemorrhage. Combinational hemorrhages may occur during injury, surgery, stroke, trauma, or through genetic and acquired platelet function disorders [4]–[13]. The outcome of a hemorrhage varies, depending on its severity; it can range from no apparent damage to severe disability [2, 3, 9, 12]. Severe bleeding can be life threatening if not treated swiftly [1, 2, 12]. Hemorrhage during trauma is a significant challenge, accounting for 30–40% of all fatalities, second only to central nervous system injury as a cause of death on battlefields [3]. However, hemorrhagic death is the leading preventable cause of mortality in combat casualties and typically occurs within 6–24 h of injury [3]. Preventing major bleeding should take priority over other conditions, except for failure of the heart or lungs. Timely intervention can save lives of injured subjects, suspend bleeding, relieve symptoms and prevent complications [1]–[13].

The demand in new methods and devices intended to effectively prevent bleeding to save patients and injured soldiers, remains high. The majority of patients with potentially survivable combat-related injuries eventually die from hemorrhage [2]. New devices will decrease combat-related casualties involving severe trauma and massive transfusion [2, 3].

Plasma devices for such applications have already been introduced. The argon plasma coagulator (APC) is a high-frequency monopolar device used for non-contact thermal coagulation. This device is used, in particular, in endoscope surgery for bleeding control [14]–[16]. The high-frequency discharge between the tip of a probe and the target tissue produces plasma in a jet of argon gas that is directed through a probe passing through the endoscope. The heat carried by the produced argon plasma cauterizes and desiccates

blood. The drawback of this treatment is the thermal damage caused on tissue surrounding the wound. Moreover, for treating larger external wounds, new devices that can deliver copious low temperature plasma would be desirable. Low temperature plasma that induces blood clotting may resolve the thermal damage problem. Kalghatgi *et al* [17] showed that a blood sample could indeed be clotted by direct contact of the sample to non-thermal atmospheric pressure plasma [18], produced by a dielectric barrier discharge (DBD).

Ambrosio *et al* [19] suggested that reactive oxygen metabolites might affect thrombus formation within the vasculature. In addition, hydrogen peroxide ( $\text{H}_2\text{O}_2$ ), a non-radical yet oxidant species, is known to play a special role in platelet agglomeration [20, 21]. Studies have shown that platelets are a prime target for oxidants produced or released in the vascular lumen. Oxidants can affect several key steps of platelet function to indirectly enhance platelet agglomeration through local increases in platelet-activating factor (PAF) [22]. Furthermore, oxidants promote *de novo* synthesis of tissue factor pro-coagulant activity [23].

A portable handheld air plasma torch (APT) is designed for large area blood coagulation applications. This torch produces low temperature ( $<75^\circ\text{C}$ ) non-equilibrium plasma in the open region, which carries abundant reactive atomic oxygen (RAO) in its effluent. RAO is capable of destroying a broad spectrum of microbes for sterilization applications [24]. Moreover, RAO gives rise to  $\text{H}_2\text{O}_2$  and oxidant hydroxyl radicals (OH) in the blood through chemical reactions.

This work aims to examine the effectiveness of APT on coagulation applications and to study the role of RAO on morphological changes of blood cells before and after plasma exposure. In pursuit of this aim, we have performed blood cell staining, optical microscopy and histological examination for morphological studies of untreated and post-exposed blood samples. The electric characteristics of the discharge for plasma generation and the spatial distribution of the 777.4 nm emissions of the torch, a signature of the generation and distribution of atomic oxygen in the plasma effluent, are presented in section 2. The preparation of the experiments is described in section 3. Experiments and the results of analysis are presented in section 4. A coagulation mechanism is presented in section 5. Discussions of the work are given in section 6.

## 2. Portable APT

### 2.1. Physical and electric characteristics

The torch device, which is handheld, uses only airflow delivered by a centrifugal fan. The airflow speed at the nozzle exit of the torch was measured by an Air Velocity Meter (tsi model 1650). The airflow rate was then estimated from integrating the speed distribution over the cross section of the nozzle. The airflow rate and average flow speed at the nozzle exit of the torch were determined to be about  $2.45 \text{ l s}^{-1}$  and  $12 \text{ m s}^{-1}$ , respectively. This torch consists of a pair of concentric electrodes and a ring-shaped permanent magnet placed concentrically below the electrodes. A schematic of the torch is presented in figure 1(a), in which the relevant dimensions are given. As shown, the gap between the electrodes is 1 mm, the ring magnet ( $12 \text{ (od)} \times 5.3 \text{ (id)} \times 6 \text{ mm}$ ) is placed at 10 mm below the gap of the electrodes and the nozzle exit is 12.5 mm above the discharge gap. The nozzle directs the flow of the plasma effluent as well as covers the electrodes for safety. The flow speed at the gap of the electrodes was estimated to be about  $25 \text{ m s}^{-1}$ . The time varying voltage  $V(t)$  and current  $I(t)$  of the discharge between the electrodes were measured using a digital oscilloscope (Tektronix TDS3012 DPO 100 MHz and  $1.25 \text{ GS s}^{-1}$ ), where  $V$  is the voltage of the central electrode of the torch (the outer

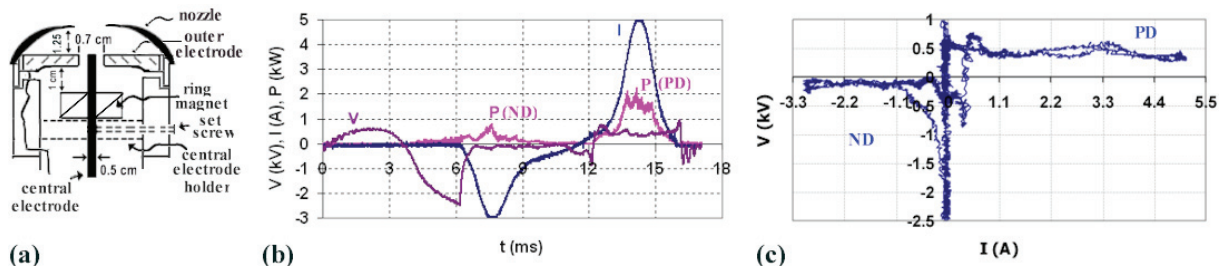


**Figure 1.** (a) A schematic of the torch, (b) voltage  $V$ , current  $I$  and power  $P$  functions of the discharge in one cycle and (c)  $V-I$  characteristic of the discharge.

electrode is grounded). Current  $I$  was measured by a current loop (0.1 V/1 A rating) around the electric wire connected to the outer electrode. The product of the  $V$  and  $I$  functions gives the instantaneous power function  $P(t)$ . These three time functions,  $V$ ,  $I$  and  $P$ , as well as the  $V-I$  characteristic are presented together in figures 1(b) and (c) to show their phase relationship. The discharge is periodic at 60 Hz and in each ac cycle there are two discharges.

As shown, the positive discharge (PD) and negative discharge (ND) are quite different in their characteristics. The peak power in the PD reaches 2 kW; however, the overall average power is about 350 W. The volume of the plasma torch is estimated to be  $10^{-5} \text{ m}^3$  (i.e.  $2 \times 10^{-6} \text{ m}^3$  inside the nozzle and  $8 \times 10^{-6} \text{ m}^3$  outside the nozzle); thus, the average power density is about  $35 \text{ MW m}^{-3}$ .

The  $V-I$  characteristic showing negative differential resistance indicates that the discharge is in arc mode; however, the arc is prevented from constriction by the introduced airflow as well as by the magnetic field of a ring-shaped permanent magnet (0.18 T at its center), which rotate the discharge to prevent the formation of hot spots on the electrodes. The airflow pushes the discharge into a loop, which protrudes to the outside of the nozzle and rotates around the axis of the central electrode by the magnetic field of the ring magnet.

We note that there are no existing models for the discharge in the presence of magnetic field. The models developed for stationary arcs in the absence of magnetic field are not completely applicable because the equation of energy balance is different and the boundary conditions inadequate. Moreover, in the presence of magnetic field, heat transfer is more complex due to arc rotation with angular speed comparable to the flow speed. Therefore, the gas temperature of the discharge in the two situations, without and with magnetic field, can be quite different. The simulation results [25] show that the gas temperature in a stationary dc discharge can reach a few thousand kelvin. On the other hand, the present torch produces rotating arc in periodic discharges; the gas temperature is less than 350 K, which is much lower than the excitation temperature of electrons channeled by the rotating arc loop.

## 2.2. Temperature measurements

The average temperature of the plasma effluent outside the nozzle was measured along the axis by a temperature meter ‘Omega DP460’ (Omega Engineering, Inc., Stamford, CT). The response time of the thermocouple of the meter is about 0.5 s. The torch was run in periodic mode with a duty cycle of about 25%. We have exposed the probe to the torch at each location to obtain a steady state reading from the meter. The time-averaged temperature distribution was



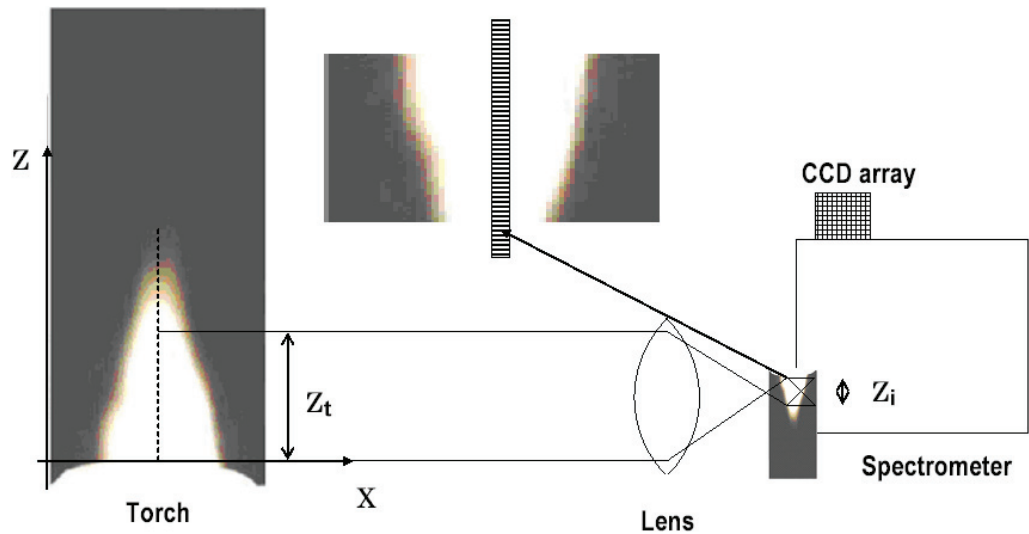


**Figure 2.** Scheme of the imaging spectroscopy.

determined from the readings. Although the size of the thermocouple was too large to provide a good spatial resolution, the measurement showed that the temperature of the plasma effluent was less than 75 °C (348 K).

Shown in figure 2 is the scheme of the imaging spectroscopy used to determine axial distribution of the electron excitation temperature  $T_{\text{exc}}(z)$  in torch plasma. The image of the torch was projected to the entrance plane of the imaging spectrometer, with magnification  $s = z_i/z_t = 0.08$ . The entrance slit cut through the central axis of the torch image. The CCD array detector captured the spectrally dispersed image of the irradiated slit image, which was then analyzed row by row to obtain individual spectral intensities  $I(z, \lambda)$ . Given the magnification factors and the size of single pixel of 25  $\mu\text{m}$ ,  $I(z, \lambda)$  corresponded to an average intensity radiated from a plasma cylinder 0.3 mm high and 0.1 mm wide cutting through the central axis of the torch. Each spectral frame was calibrated using a black body radiation source to eliminate the error induced by the grating position.

The recorded spectrum is abundant in Cu I lines. To determine the electron excitation temperature, we have chosen some of the lines that correspond to transition to the ground state, since they are best documented. Seven lines, at 216.509, 217.894, 222.57, 249.215, 324.754 and 327.396 nm, respectively, are included in the Boltzmann plot according to the relation

$$I(z, \lambda)\lambda/g_k A_{ki} = C \times \exp[-E_k/kT_{\text{exc}}(z)], \quad (1)$$

where  $I(z, \lambda)$  is the measured intensity of the spectral line of wavelength  $\lambda$ ,  $g_k$  is the statistical weight of the upper state in the transition with probability  $A_{ki}$ ,  $E_k$  is the energy gap in the transition,  $k$  is the Boltzmann constant and  $T_{\text{exc}}(z)$  is the electron excitation temperature at vertical position  $z$  with respect to the torch baseline (cap surface or electrode surface). Electron excitation temperature  $T_{\text{exc}}(z)$  is then obtained by plotting the normalized spectral line intensity (left side of equation (1)) as a function of the energy of the transition  $E_k$ , and by fitting to the exponential function and evaluating the optimum coefficient in the exponent. The result is presented in figure 3. As shown, the electron excitation temperature is about 7500 K. Atomic levels used in excitation temperature evaluation had ionization energy of the order of 1–4 eV.



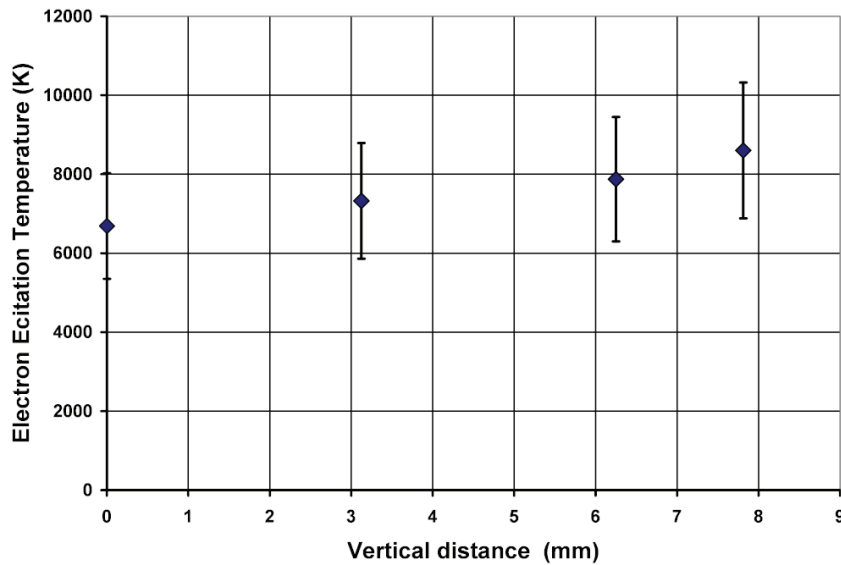


**Figure 3.** Axial distribution of the electron excitation temperature.

One can estimate then that the average electron energy in the non-thermal component of the electron plasma is of the order of several electron volts.

### 2.3. Emission spectroscopy

The spatial distribution of the 777.4 nm emissions from the 5P state of RAO in the plasma effluent of the torch was measured. The image data from the entire plasma plume could be taken simultaneously with an Apogee Alta E47 thermoelectrically cooled CCD camera with a Nikon 50 mm f/1.2 lens and a 50 mm diameter 10 nm pass band interference filter with a center wavelength of 780 nm. However, due to the short lifetime ( $\sim 0.2\text{--}0.3$  ms) of atomic oxygen [26], the axial distribution of the emission intensity was expected to vary strongly and to have a sharp upward extent. To capture the full axial extent of this distribution beyond the dynamic range of a single 16-bit digital image, multiple images of the torch were recorded separately with a moveable stage approximately 0.15 m square draped in black velvet cloth blocking the brighter portions of the torch to allow operation of the camera at higher sensitivity and longer exposure times while avoiding saturation in the brighter parts of the torch flame. The resulting images were then calibrated and combined into a composite image giving contours of the intensity distribution, ranging from  $10^5$  to  $10^9$  Rayleighs, as shown in figure 4. An image of the plasma plume of the torch recorded by a video camera is included on the right-hand side in figure 4 for reference. As shown, the visible plasma plume extends out axially to about 30 mm from the nozzle exit of the torch, where the intensity of 777.4 nm emissions is about  $10^5$  Rayleigh; i.e. the total photon emission from a slice of the torch at 30 mm away from the nozzle is about  $10^{15} \text{ m}^{-2} \text{ s}^{-1}$ . The corresponding density and flux of RAO at 5P state are estimated to be about  $3 \times 10^{12} \text{ m}^{-3}$  and  $6 \times 10^{13} \text{ m}^{-2} \text{ s}^{-1}$ , respectively.

There are two likely processes to produce atomic oxygen; one is through recombination of charged particles, which may not need the presence of energetic electrons. The produced atomic oxygen is most likely in the ground state, which cannot be identified via emission spectroscopy. The other one is to dissociate an oxygen molecule into two oxygen atoms via the reaction

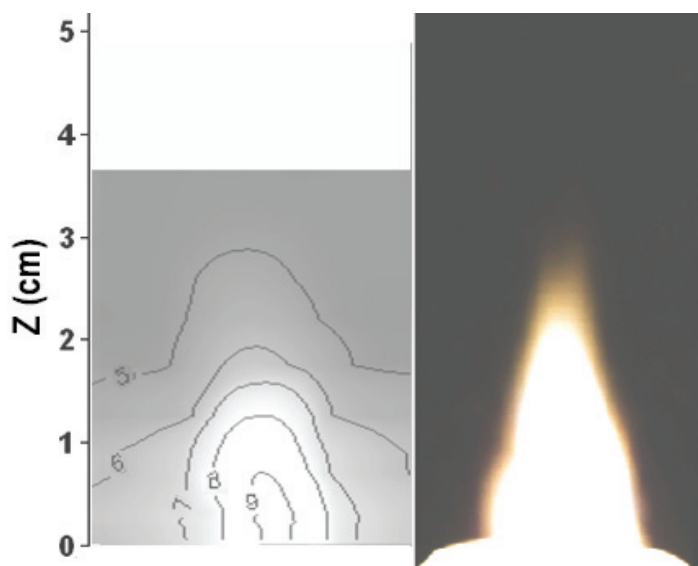


**Figure 4.** The spatial distribution of the emission intensity at 777.4 nm of the torch; the numerical value at each contour is the  $\log_{10}$  of the intensity in Rayleigh; a video graph of the plasma plume is also included.

$e^- + O_2 \rightarrow 2O + e^-$ , which has a reaction rate coefficient  $k_1 = 4.2 \times 10^{-9} e^{-5.6/T_e}$  [27], where  $T_e$  is in electron volts. This reaction rate decreases rapidly with  $T_e < 5.6$  eV; thus it needs about 5 eV electrons to effectively dissociate  $O_2$  into atomic oxygen. Because the 5P state of the transition in RAO has rather high energy relative to the ground state, about 10.74 eV, the strong line intensity at 777.4 nm outside the core of the torch (i.e. outside the white area of the contour plot) indicates that there is a strong presence of high-energy electrons ( $>10$  eV) in the plasma effluent. The excitation temperature of 7500 K and a strong presence of  $>10$  eV electrons infer that the plasma torch is non-equilibrium; it carries a considerable amount of energetic electrons ( $>5$  eV), which are able to dissociate oxygen molecules into oxygen atoms.

As shown by Namihira *et al* [28], NO was produced in room air using a pulsed arc discharge, which generated discharge plasma having temperatures higher than 9000 K. Thus, the scheme of the imaging spectroscopy shown in figure 2 was used to detect the NO lines peaking at 239 nm (overlapped  $Q_1(12.5)$  and  $Q_2(19.5)$  transitions in the  $\delta(0, 0)$  band). The setup was also used to detect OH lines occurring between 306 and 310 nm. These lines with significant intensities were indeed detected in the region close to the electrodes (i.e. inside the nozzle) which were hot; but their intensities outside the nozzle reduced to insignificant levels. This is consistent with the fact that the temperatures of the electrodes are much higher than the gas temperature outside the nozzle that introduces a buffer distance of 12.5 mm; and NO and OH formations were strongly associated with the temperature of the plasma. The RAO lines at 777.4 nm inside the nozzle were significantly quenched by the presence of NO and OH. On the other hand, significant photon flux at 777.4 nm were detected outside the nozzle (by a CCD camera affiliated with a pass band interference filter) as shown in figure 4. The spectrometer (figure 2) also scanned the emission spectrum of the torch outside the nozzle from 300 to 900 nm. In this spectral range, intensive lines contributed by oxygen radicals appear only around 777.4 nm, confirming that the photon flux passing through the 10 nm pass band

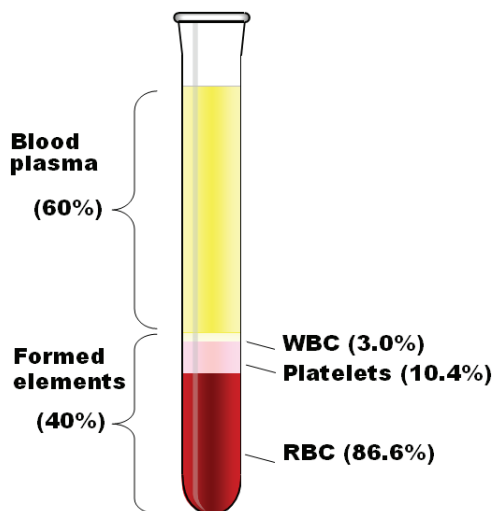


**Figure 5.** Composition of whole blood: blood plasma and formed elements.

interference filter with a center wavelength of 780 nm corresponds to the RAO lines. The UV radiation from 300 to 400 nm was not detected.

### 3. Preparations

#### 3.1. Materials

Water W3500 tissue culture grade glass slides were purchased from Sigma-Aldrich (St. Louis, MO). Blood samples were obtained from volunteers at the New York University (NYU) School of Medicine, New York, NY.

#### 3.2. Preparations prior to plasma exposure

All experiments involving blood handling, plasma torch treated samples were carried out at the Polytechnic Institute of NYU, Brooklyn, NY. Whole blood, blood plasma and formed elements were used for experiments. As shown in figure 5, blood is a fluid tissue that includes 60% of a liquid portion known as blood plasma and 40% of formed elements or blood cells [29]. Blood plasma is the liquid portion of the blood—a protein–salt solution that suspends red blood cells (RBC), white blood cells (WBC) and platelets alike. Formed elements consist 86.6% of RBC, 10.4% of platelets and 3% of WBC. The latter is comprised of neutrophils, eosinophils, basophils, monocytes and lymphocytes [29].

In order to prevent premature blood coagulation, obtained blood was mixed with a 3.2% sodium citrate solution on a 9 : 1 ratio (in volume). The sodium citrate solution is a commonly used reagent to prevent blood from clotting by chelating calcium ions [30, 31]. In addition, anti-coagulated blood samples were left sitting for 3–5 min at room temperature allowing the blood samples to separate into two fractions including (i) blood plasma (upper) and (ii) formed elements (lower) (see figure 5), respectively. Blood smears were prepared from whole blood, blood plasma and formed elements according to a previously established protocol [32]. Samples were further treated using the procedure as described in section 3.3.

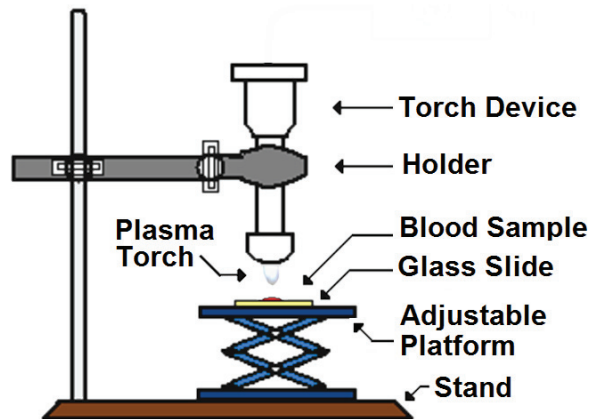


**Figure 6.** Schematic of the experimental setup.

### 3.3. Experimental setup

A portable APT was secured on a fixed cross holder with its 20-mm-diameter circular nozzle exit facing downwards. A jack directly below the nozzle exit was used to position the sample plate below the APT nozzle. Two vertical distances of 25 and 40 mm, and exposure times of 2–10 s for blood-smear samples ( $5.0 \mu\text{l}$ ) and 4–16 s for blood plasma/formed elements-smear samples ( $5.0 \mu\text{l}$ ) were chosen in the tests. In the tests involving droplet-samples ( $10.0 \mu\text{l}$ ), the exposure distances of 25, 30 and 40 mm and exposure times of 8 and 16 s were chosen. The torch plasma effluent was directed downwards onto the sample plate placed on the platform. A schematic of the experimental setting is presented in figure 6.

### 3.4. Microscopy of plasma treated samples

Untreated (control) and plasma torch-treated smear samples from section 3.3 were subject to further cell staining and microscopy analysis at the University of Arkansas at Little Rock, Little Rock, AR. Sample staining was performed under a Biological Safety Cabinet Class IIA/B3 Forma Scientific Inc. (Marjetta, OH). Staining of untreated smear (control) and plasma torch-treated smear samples was performed using a three-step procedure using the Neat Stain Hematology kit (Astral Diagnostics Inc., West Deptford, NJ). This procedure allowed distinguishing RBC, WBC and platelets in smear samples using either whole blood, blood plasma or formed elements (figure 5). Briefly, each glass slide harboring a smear sample was dipped five times into a fixative solution, for 1 s each time. The excess reagent was then drained. The glass slides were then dipped into solutions I and II, rinsed with deionized water and later dried. All stained samples were examined at a magnification of  $200\times$  using a Nikon Eclipse E400 POL polarizing optical microscope (Nikon Corp., Japan) coupled to a CCD camera, Model 3.2.0 (Diagnostics, Instruments, Inc. USA). Digital micrographs of samples were acquired in real-time. Five determinations were made for each sample. RBC, WBC and platelets were identified and counted using the standard procedure as previously described [33].

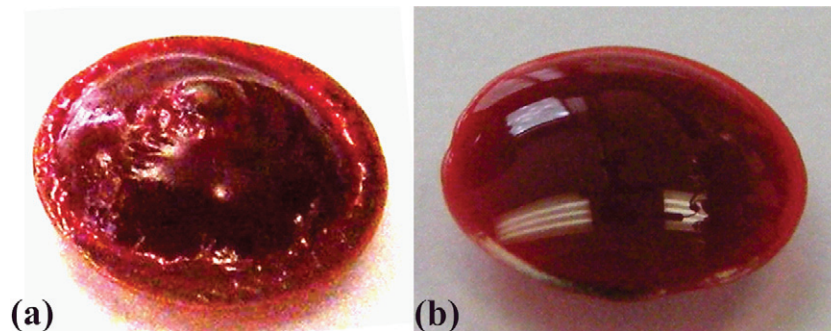


**Figure 7.** Blood samples treated by (a) the plasma effluent of the torch and (b) a heated airflow.

#### 4. Experiments

Two tests to separate the effects of heat and torch plasma effluent (oxygen radicals) on blood clotting were performed first. Test 1 was performed with a blood droplet set on a glass slide, placed at 25 mm below the torch nozzle to be directly exposed to the plasma effluent. Direct exposure treatment continued for a period of 12 s. The sample temperature rose to 52 °C. The result of the test is presented in figure 7(a). A shell, formed on the blood sample surface, can be clearly seen. In the second test, a blood droplet was set in a well and treated for 16 s by the hot airflow of a hair dryer, which raised the sample temperature to about 61 °C. A photo of the sample taken after this hot air treatment is presented in figure 7(b) for a comparison. No noticeable blood clotting can be identified. This comparison clearly shows that the blood coagulation appearing in figure 7(a) cannot be attributable to thermal effect of hot air.

We next examined the dependence of coagulation on the reactive oxygen species (ROS) flux (mainly RAO indicated by the emission spectroscopy) in the plasma effluent by fixing the exposure times to 16 s. The tests were conducted at three exposure distances, namely 25, 30 and 40 mm. The exposure times of 16 s in each test were, in fact, accumulations of 4 s exposures with a 2 s pause after two consecutive 4 s exposures. The sample temperatures rose to about 50 °C in all three tests. Although all treated samples, presented in figure 8, manifested blood clotting, as evidenced by shell formation on the blood sample surfaces, the degree of blood clotting differs as the dissimilar blood sample surface structure led to conclude. As the degree of dryness and hardness of a shell increases, the bubble on that shell surface tends to collapse and consequently forms dimples. As seen in figure 8(c), the shell is smoother than the other two shown in figures 8(a) and (b). Furthermore, the bubble of the shell in figure 8(a) appears collapsed. Results show that the degree of blood clotting decreases with increasing exposure distance. This tendency is consistent with the decrease of the RAO flux in the plasma effluent with increasing exposure distance. Three treated samples, with exposure times of 8, 12 and 16 s, are presented in figure 9 to demonstrate that the degree of blood clotting increases with exposure time, with a constant exposure distance of 25 mm.

Another test was performed using whole blood, blood plasma and formed elements (figure 10). Untreated blood samples were used as control (row 1, figure 10). The exposure distance and time were 30 mm and 16 s, respectively. The test results are presented in row 2 of figure 10 for treated whole blood (panel 2(a)), blood plasma (panel 2(b)) and formed elements droplet-samples (panel 2(c)). Digital micrographs of untreated controls (panel 3(a)) and





**Figure 8.** Samples treated with a total of 16 s exposure time (4 s exposures, with a 2 s pause between two consecutive exposures) at three exposure distances, namely (a) 25 mm, (b) 30 mm and (c) 40 mm.

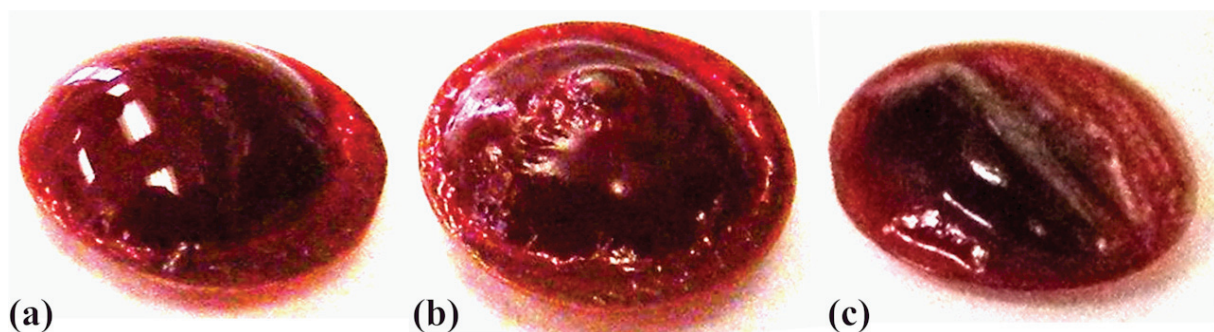


**Figure 9.** Samples treated at three exposure times (a) 8 s, (b) 12 s and (c) 16 s; with a fixed exposure distance of 25 mm.

plasma-treated samples (panels 3(b) and (c)) are presented as well. A dark brown shell, manifesting blood clotting, can be seen in the whole blood and formed elements samples but is not observed in the treated blood plasma sample. The treated formed elements (figure 10, panel 2(c)) sample appears darker. The sample is found dryer and harder compared to the treated whole blood sample (figure 10, panel 2(a)).

## 5. Coagulation mechanism

Formed elements and blood plasma contribute to blood coagulation during hemorrhage. Blood plasma contains albumin (the chief protein constituent), fibrinogen (responsible, in part for blood clotting), globulins (including antibodies) and other clotting proteins [29]. RBC contains hemoglobin, a complex iron-containing protein that carries oxygen and participates in carbon dioxide exchange. Platelets play a vital role in the early response to vascular injury and blood clot formation as they adhere to injured vessel wall components, become activated, agglomerate and secrete mediators that promote platelet activation and attract WBC [34]–[36]. The average lifetime for WBC is hours to days, for RBC 120 days and for platelets 9 days. Platelets are more fragile cells and 3–4 times smaller than RBC [29, 37, 38].

Microscopy and cell count were performed on both control and plasma torch-treated blood samples. Percentages of RBC, WBC and platelets in the total cell count of each sample were evaluated. We did not find any deviating values for WBC. The latter consists of only 3% in healthy blood [29].

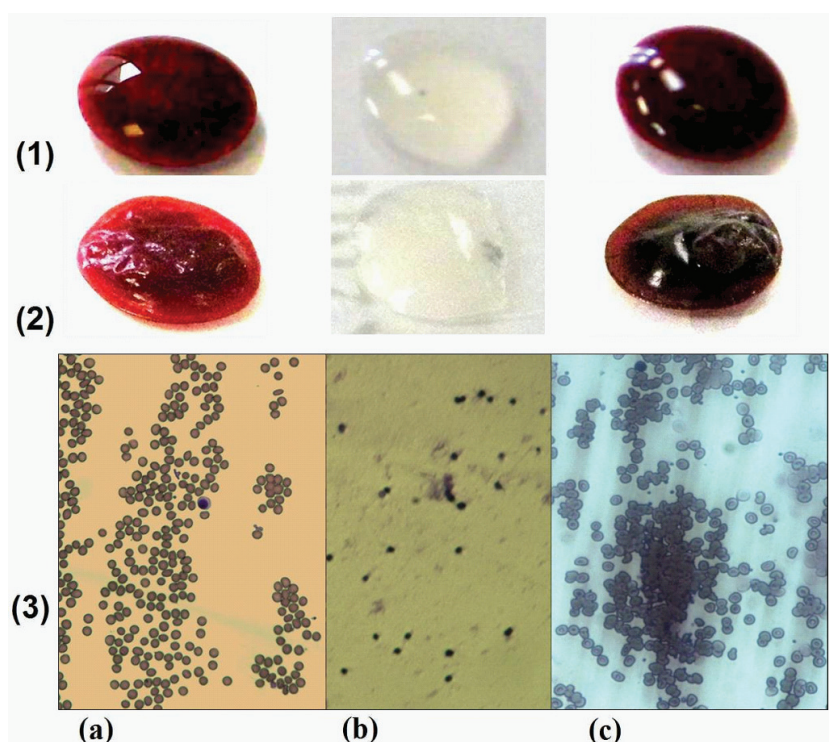


**Figure 10.** Untreated control (line 1) and plasma-torch treated samples (line 2) including whole blood (2a), blood plasma (2b) and formed elements (2c). Digital micrographs of untreated whole blood sample (3a), blood plasma (3b) and formed elements (3c) are shown.

In addition, our results revealed that in the sample treated with longer exposure time and shorter exposure distance, the percentage of RBC increased, while the percentage of the platelets decreased. These two dependences on exposure distance and time are shown in figures 11 and 12, respectively. This was confirmed by identification of cell types using cell staining and cell counts. The significant reduction of the percentage of platelets of the treated sample was evidence of the impact of the plasma effluent on platelets; in particular, because RBC concentration should not change much, it is suggested that, in fact, the platelet count of the treated sample was reduced.

As shown in figure 8, blood clotting decreases with the increase of exposure distance. Likewise, as shown in figure 4, RAO carried by the plasma effluent of the torch also decreases with increasing exposure distance.

The experimentally observed dependencies can be summarized as follows. With an increase of the exposure distance, the platelet count of treated samples increases, but is less than that of the control (figure 11). The RAO flux as well as blood clotting decrease (figure 8). With an increase in exposure time, platelet count of treated samples decreases (figure 12), while blood clotting increases (figure 9). These correlations lead us to propose a blood clotting mechanism as shown in figure 13.

The cartoon plots in figure 13 are used to explain the plasma torch coagulation mechanism. Presumably, RAO in the plasma effluent creates oxidants, such as  $H_2O_2$  and  $OH$ , in the blood. These oxidants contribute to RBC–platelets and WBC interactions (figure 13(a)), which



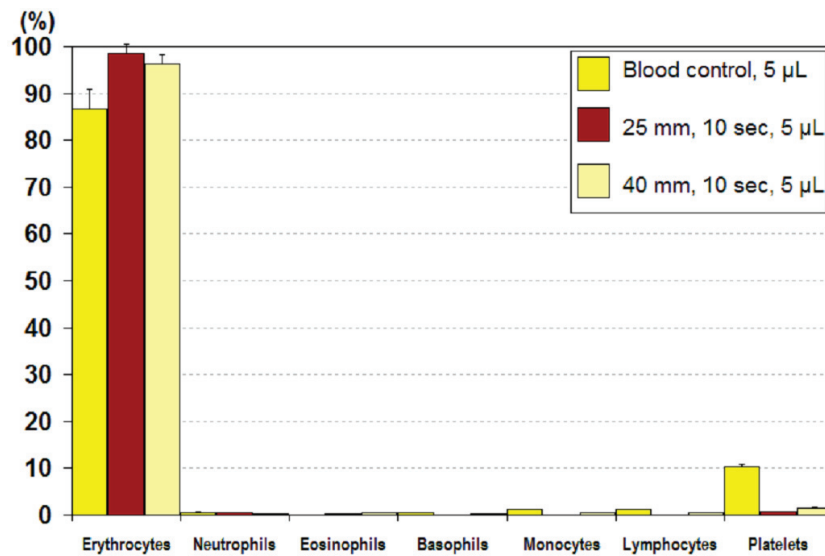


**Figure 11.** Relationship between the blood composition of untreated/plasma-treated samples and the exposure distance; the exposure time is 10 s.

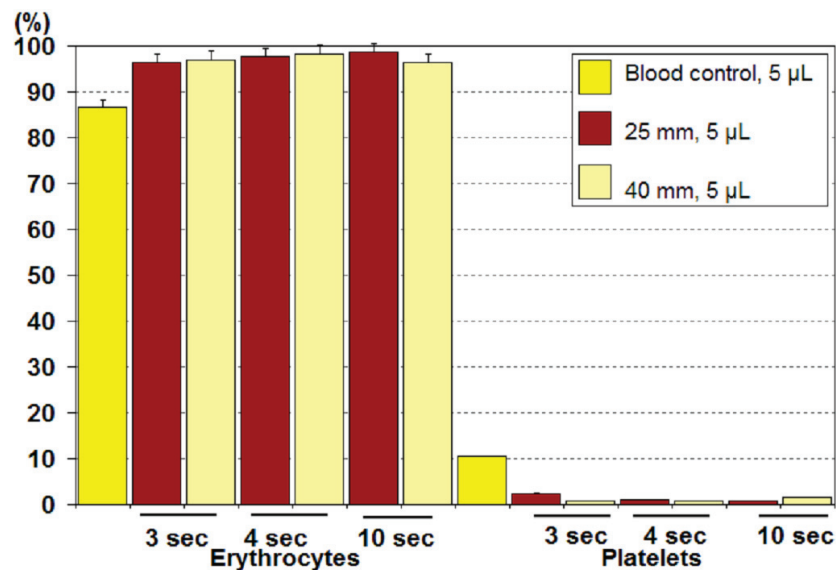


**Figure 12.** Relationship between blood composition of untreated/plasma-treated samples and the exposure time at two exposure distances, 25 and 40 mm.

in return causes a noticeable decrease in blood flowability. These interactions influence the concentration of cells suspended in blood (figure 13(b)). The increase of RBC can be observed under the microscope. Consequently, coagulation is on the rise, while platelets are decreasing. This is due to trapping within globular complexes (figure 13(c)). Evidence points to RBC that trigger platelet adherence/agglomeration *in vitro*, as well as blood clotting [39]–[42]. It was shown that platelet agglomeration was associated with the loss of adenine nucleotides released by RBC [43], the extent of which increased together with RBC [44]. In addition to blood

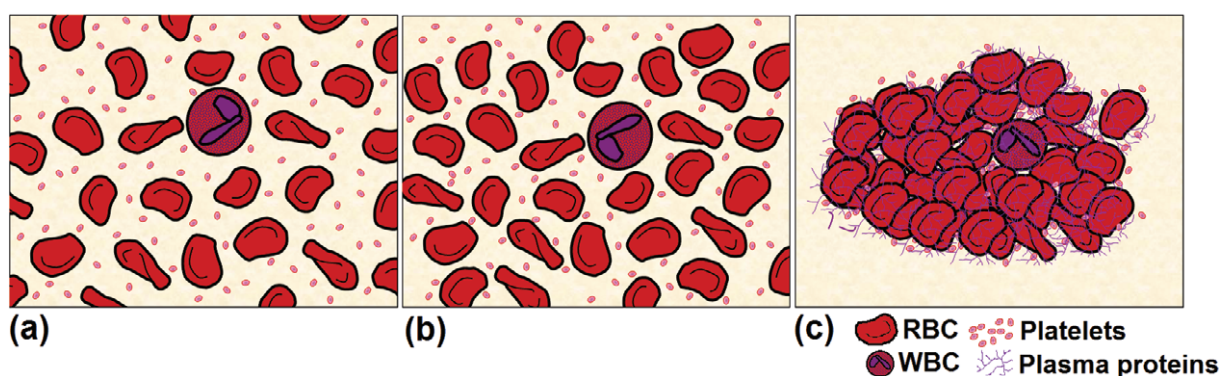


**Figure 13.** Cartoon plots showing the clotting process induced by the plasma torch.

clotting, which transiently stops bleeding, platelets provide a surface for the subsequent steps of the coagulation leading to clot formation [35, 36]. Additionally, platelets are fragmented by oxidants to induce coagulation and subsequent blood clot formation (figure 13). Viscosity of blood samples will also be affected by oxidants that presumably contribute to the denaturation of albumin [45] as well as other proteins found in the blood. Taken together, our results demonstrate that the plasma torch induces coagulation with the involvement of RBC, platelets (figure 13), and most likely albumin. Prospective studies on RBC only or platelets only and/or platelets/albumin enriched/depleted samples will confirm our current findings.

NO can lead to anti-inflammation and anti-thrombotic effects that inhibit platelet adhesion, increases blood flowability and lowers blood pressure [46]. It was demonstrated that NO containing drugs such as an NO donor (e.g. nitroglycerin) or NO inhalant, inhibit platelet agglomeration [46]–[53]. NO suppresses platelet agglomeration *in vitro* and *in vivo* via the guanylyl cyclase mechanism [48]–[53]. Furthermore, exposure to inhaled NO significantly decreases platelet agglomeration in rats [51] and in humans accompanied by acute respiratory distress syndrome [46, 47]. The present torch operates at a relatively low temperature ( $<75^{\circ}\text{C}$  outside the nozzle). The NO flux in the plasma effluent outside the nozzle is relatively low and does not significantly quench the effect of RAO involved in platelet agglomeration and inducing blood coagulation.

It is noted that other ROS, in addition to RAO, can also create oxidants in the blood to induce coagulation via the proposed mechanism. In the scan of the spectrometer, intensive lines contributed by oxygen radicals appeared only around 777.4 nm. However, it could be because the emissions of molecule species were distributed in the bands with much lower spectral intensities. Given the limitations of spectroscopic diagnostics, we could not rule out the existence of other ROS in the torch, which were also partially responsible for the observed coagulation.

## 6. Discussion

The present experiment shows that a low temperature plasma torch can rapidly clot blood. Although both RAO and NO are generated within the plasma effluent of the torch, the experimental results presented in this paper are more consistent with the published data on the effect of oxidants on blood coagulation. Therefore, the clotting process should be attributed

to the stimulation of RBC–platelets and/or WBC interactions by the oxidants created during the interaction of blood and RAO (as well as other likely ROS). However, further confirmation by prospective studies is still needed because the contribution of NO to blood coagulation, although controversial in the literature, cannot be ruled out completely.

Prospective studies will focus on how ROS and NO produced by the plasma torch influence each individual cell type using only a single cell type, either RBC, WBC, or platelets, in order to verify their actual involvement in blood clotting, blood coagulation and fibrinolysis. Moreover, although results from the present study are promising, the tests were performed in well-controlled *in vitro* conditions and might not be directly extrapolated to the much more complicated *in vivo* environment. Therefore, the usefulness of the plasma torch on *in vivo* blood coagulation will also need to be further studied and validated.

The present studies could lead to the development of a portable device triggering blood clotting that can be implemented in emergency rooms, ambulances or on battlefields.

## Acknowledgments

We extend our sincere appreciation to Dr Shiaoqing Gong of the Rockefeller University for her technical support of the blood-coagulation experiment and insightful discussion on the experimental results. We also thank Alessandro Betti for putting together the plasma torch device. This work was supported in part by a NYU-Poly seed Grant and Adventix Technologies Inc.

## References

- [1] Jevon P and Cooper L 2008 First aid. Part 5: First-aid treatment for severe bleeding *Nurs. Times* **104** 26–7
- [2] Spinella P C, Perkins J G, McLaughlin D F, Niles S E, Grathwohl K W, Beekley A C, Salinas J, Mehta S, Wade C E and Holcomb J B 2008 The effect of recombinant activated factor VII on mortality in combat-related casualties with severe trauma and massive transfusion *J. Trauma* **64** 286–94
- [3] Perkins J G, Cap A P, Weiss B M, Reid T J and Bolan C D 2008 Massive transfusion and nonsurgical hemostatic agents *Crit. Care Med.* **36** (Suppl 7) S325–39
- [4] Scharf R E 2008 Acquired platelet function disorders: pathogenesis, classification, frequency, diagnosis, clinical management *Hamostaseologie* **28** 299–311
- [5] Trouillas P and von Kummer R 2006 Classification and aetiology of cerebral hemorrhages after thrombolysis in ischemic stroke *Stroke* **37** 556–61
- [6] Franchini M 2008 Surgical prophylaxis in von Willebrand's disease: a difficult balance to manage *Blood Transfus.* **6** (Suppl 2) s33–8
- [7] Al-Sallami H, Ferguson R, Wilkins G, Gray A and Medlicott N J 2008 Bleeding events in patients receiving enoxaparin for the management of non-ST-elevation acute coronary syndrome (NSTEACS) at Dunedin Public Hospital, New Zealand *N. Z. Med. J.* **121** 87–95
- [8] Roy P *et al* 2008 Impact of 'nuisance' bleeding on clopidogrel compliance in patients undergoing intra-coronary drug-eluting stent implantation *Am. J. Cardiol.* **102** 1614–7
- [9] Milovanov A P and Kirsanov IaN 2008 The pathogenesis of uterine hemorrhages in the so-called placental polyps *Arkh. Patol.* **70** 34–7
- [10] Jamal M M, Samarasena J B and Hashemzadeh M 2008 Decreasing in-hospital mortality for oesophageal variceal hemorrhage in the USA *Eur. J. Gastroenterol. Hepatol.* **20** 947–55
- [11] Thanvi B R, Treadwell S and Robinson T 2008 Haemorrhagic transformation in acute ischaemic stroke following thrombolysis therapy: classification, pathogenesis and risk factors *Postgrad. Med. J.* **84** 361–7

- [12] Kramer A H, Gurka M J, Nathan B, Dumont A S, Kassell N F and Bleck T P 2008 Complications associated with anemia and blood transfusion in patients with aneurysmal subarachnoid hemorrhage *Crit. Care Med.* **36** 2070–5
- [13] Derex L and Nighoghossian N 2008 Intracerebral haemorrhage after thrombolysis for acute ischaemic stroke: an update *J. Neurol. Neurosurg. Psychiatry.* **79** 1093–9
- [14] Vargo J J 2004 Clinical applications of the argon plasma coagulator *Gastrointest. Endosc.* **59** 81–88
- [15] Raiser J and Zenker M 2006 Argon plasma coagulation for open surgical and endoscopic applications: state of the art *J. Phys. D: Appl. Phys.* **39** 3520–3
- [16] Malick K J 2006 Clinical applications of argon plasma coagulation in endoscopy *Gastroenterol. Nur.* **29** 386–91
- [17] Kalghatgi S U, Fridman G, Cooper M, Nagaraj G, Peddinghaus M, Balasubramanian M, Vasilets V N, Gutsol A F, Fridman A and Friedman G 2007 Mechanism of blood coagulation by nonthermal atmospheric pressure dielectric barrier discharge plasma *IEEE Trans. Plasma Sci.* **35** 1559–66
- [18] Fridman G, Peddinghaus M, Ayan H, Fridman A, Balasubramanian M, Gutsol A, Brooks A D and Friedman G 2006 Blood coagulation and living tissue sterilization by floating electrode dielectric barrier discharge in air *Plasma Chem Plasma Process* **26** 425–42
- [19] Ambrosio G, Tritto I and Golino P 1997 Reactive oxygen metabolites and arterial thrombosis *Cardiovasc. Res.* **34** 445–52
- [20] Del Principe D, Menichelli A, De Matteis W, Di Giulio S, Giordani M, Savini I and Finazzi-Agro A 1991 Hydrogen peroxide is an intermediate in the platelet activation cascade triggered by collagen, but not by thrombin *Thromb. Res.* **62** 365–75
- [21] Del Principe D, Menichelli A, De Matteis W, Di Corpo M L, Di Giulio S and Finazzi-Agro A 1985 Hydrogen peroxide has a role in the aggregation of human Platelets *FEBS Lett.* **185** 142–6
- [22] Ambrosio G, Oriente A, Napoli C, Palumbo G, Chiariello P, Marone G, Condorelli M, Chiariello M and Triggiani M 1994 Oxygen radicals inhibit human plasma acetylhydrolase, the enzyme that catabolizes platelet-activating factor *J. Clin. Invest.* **93** 2408–16
- [23] Golino P *et al* 1996 Effects of tissue factor induced by oxygen free radicals on coronary flow during reperfusion *Nat. Med.* **2** 35–40
- [24] Lai W, Lai H, Kuo S P, Tarasenko O and Levon K 2005 Decontamination of biological warfare agents by a microwave plasma torch *Phys. Plasmas* **12** 23501–6
- [25] Benilov M S and Naidis G V 2003 Modelling of low-current discharges in atmospheric-pressure air taking account of non-equilibrium effects *J. Phys. D: Appl. Phys.* **36** 1834–41
- [26] Oda T, Yamashita Y, Takezawa K and Ono R 2006 Oxygen atom behavior in the nonthermal plasma *Thin Solid Films* **506–507** 669–73
- [27] Georg A, Engemann J and Brockhaus A 2002 Investigation of a pulsed oxygen microwave plasma by time-resolved two-photon allowed laser-induced fluorescence *J. Phys. D: Appl. Phys.* **35** 875–81
- [28] Namihira T, Sakai S, Matsuda M, Wang D, Kiyon T, Akiyama H, Okamoto K and Toda K 2007 Temperature and nitric oxide generation in a pulsed arc discharge plasma *Plasma Sci. Technol.* **9** 747–51
- [29] Anthea M *et al* 1993 *Human Biology and Health* (Englewood Cliffs, NJ: Prentice-Hall)
- [30] Greer J P *et al* 2003 *Wintrobe's Clinical Hematology* 11th edn (New York: Lippincott, Williams and Wilkins)
- [31] Fridman G, Shereshevsky A, Jost M M, Brooks A D, Fridman A, Gutsol A, Vasilets V and Friedman G 2007 Floating electrode dielectric barrier discharge plasma in air promoting apoptotic behavior in melanoma skin cancer cell lines *Plasma Chem. Plasma Process* **27** 163–76
- [32] Coligan E *et al* 1999 *Curr. Protocol. Immun.* (New York: Wiley)
- [33] Houwen B 2001 The differential cell count *Lab Hematol.* **7** 89–100
- [34] Reimers R C, Sutura S P and Joist H J 1984 Potentiation by red blood cells of shear-induced platelet aggregation: relative importance of chemical and physical mechanisms *Blood* **64** 1200–6
- [35] Sachs U J and Nieswandt B 2007 *In vivo* thrombus formation in murine models *Circ. Res.* **100** 979–91
- [36] Kolev K, Longstaff C and Machovich R 2005 Fibrinolysis at the fluid-solid interface of thrombi *Curr. Med. Chem. Cardiovasc. Hematol. Agents* **3** 341–55

- [37] Laura Dean Bethesda (MD) 2005 *Blood Groups and Red Cell Antigens* (National Library of Medicine (US): NCBI)
- [38] [www.genomesize.com/cellsize/mammals.htm](http://www.genomesize.com/cellsize/mammals.htm)
- [39] Machovich R and Owen W G 1990 The elastase-mediated pathway of fibrinolysis *Blood Coagul. Fibrinolysis* **1** 79–90
- [40] Born G V R, Bergquist D and Arfors K E 1976 Evidence for inhibition of platelet activation in blood by a drug effect on erythrocytes *Nature* **259** 233–35
- [41] Bergquist D and Arfors K E 1980 Haemostatic platelet plug formation in the isolated rabbit mesenteric preparation—an analysis of red blood cell participation *Thromb. Haemost.* **44** 6
- [42] Schmid-Schdnbein H *et al* 1979 *Basic Aspects of Blood Trauma* (Stuttgart: Schattauer) 322–40
- [43] Tiefenbach H-J, Durchschlag H, Schneider G and Jaenicke R 2004 Thermodynamic analysis of serum albumin denaturation by sodium dodecyl sulfate *Aqueous Polym. dispersions* **124** 130–40
- [44] Schmid-Schdnbein H, Born G V R, Richardson P D, Cusack N, Rieger H, Forst R, Rohling-Winkel J, Blasberg P and Wehmeyer A 1981 Rheology of thrombotic processes in flow: The interaction of erythrocytes and thrombocytes subjected to high flow forces *Biorheology* **18** 415–44
- [45] Meireles M, Aimar P and Sanchez V 2004 Albumin denaturation during ultrafiltration: Effects of operating conditions and consequences on membrane fouling *Biotechnol. Bioeng.* **38** 528–34
- [46] Ricciardi M J, Knight B P, Martinez F J and Rubenfire M 1998 Inhaled nitric oxide in primary hypertension: a safe and effective agent for predicting response to nifedipine *J. Am. Coll. Cardiol.* **32** 1068–73
- [47] Mathisen D J *et al* 1998 Inhaled nitric oxide for adult respiratory distress syndrome after pulmonary resection *Ann. Thorac. Surg.* **66** 1894–902
- [48] Weber A, Strobach H and Schror K 1993 Direct Inhibition of platelet function by organic nitrates via nitric oxide formation *Eur. J. Pharmacol.* **247** 29–37
- [49] Moro M A *et al* 1996 cGMP mediates the vascular and platelet actions of nitric oxide: confirmation using an inhibitor of the soluble guanylyl cyclase *Proc. Natl Acad. Sci. USA* **93** 1480–5
- [50] Aoki H *et al* 1997 Platelet function is inhibited by nitric oxide liberation during nitroglycerin-induced anaesthesia *Br. J. Anaesth.* **79** 476–81
- [51] Nong Z *et al* 1997 Nitric oxide inhalation inhibits platelet aggregation and platelet-mediated pulmonary thrombosis in rats *Circ. Res.* **81** 865–9
- [52] Brune B and Hanstein K 1998 Rapid reversibility of nitric oxide induced platelet inhibition, *Thromb. Res.* **90** 83–91
- [53] Gries A *et al* 1998 Inhaled nitric oxide inhibits human platelet aggregation P-selectin expression and fibrinogen binding *in vitro* and *in vivo*, *Circulation* **97** 1481–7